PNAS RESEARCH ARTICLE | CELL BIOLOGY

OTUB2 silencing promotes ovarian cancer via mitochondrial metabolic reprogramming and can be synthetically targeted by CA9 inhibition

Yabing Nan[a,1], Xiaowei Wu[b,c,1], Qingyu Luo[d,1], Wan Chang[a,1], Pengfei Zhao[a], Lingqiang Zhang[e], and Zhihua Liu[a,2]

Edited by Benjamin Neel, Department of Medicine, New York University, New York, NY; received September 5, 2023; accepted March 27, 2024

Ovarian cancer is an aggressive gynecological tumor characterized by a high relapse rate and chemoresistance. Ovarian cancer exhibits the cancer hallmark of elevated glycolysis, yet effective strategies targeting cancer cell metabolic reprogramming to overcome therapeutic resistance in ovarian cancer remain elusive. Here, we revealed that epigenetic silencing of Otubain 2 (*OTUB2*) is a driving force for mitochondrial metabolic reprogramming in ovarian cancer, which promotes tumorigenesis and chemoresistance. Mechanistically, OTUB2 silencing destabilizes sorting nexin 29 pseudogene 2 (SNX29P2), which subsequently prevents hypoxia-inducible factor-1 alpha (HIF-1α) from von Hippel–Lindau tumor suppressor-mediated degradation. Elevated HIF-1α activates the transcription of carbonic anhydrase 9 (*CA9*) and drives ovarian cancer progression and chemoresistance by promoting glycolysis. Importantly, pharmacological inhibition of CA9 substantially suppressed tumor growth and synergized with carboplatin in the treatment of *OTUB2*-silenced ovarian cancer. Thus, our study highlights the pivotal role of OTUB2/SNX29P2 in suppressing ovarian cancer development and proposes that targeting CA9-mediated glycolysis is an encouraging strategy for the treatment of ovarian cancer.

ovarian cancer | metabolic reprogramming | ubiquitination | tumorigenesis | chemoresistance

Ovarian cancer is the most lethal gynecological malignancy worldwide, with a mortality rate of more than 60%. According to available statistics, there were approximately 313,959 new cases of ovarian cancer and 207,252 deaths from ovarian cancer worldwide in 2020 (1). Most ovarian cancer patients are diagnosed with advanced-stage disease, for which the 5-y survival rate is only approximately 20% (2). High-grade serous ovarian cancer is the dominant pathological subtype of ovarian cancer and accounts for approximately 70 to 80% of ovarian cancer-related deaths (3). The standard regimen for ovarian cancer treatment is debulking surgery combined with platinum/taxane-based chemotherapy. Most patients initially respond well to this therapeutic strategy but ultimately experience disease relapse with chemoresistance and have a poor prognosis (4). Several targeted therapies have been proposed based on the next-generation sequencing data generated in the last decade, but the molecular mechanisms beyond the genomic level are still largely unknown. Therefore, it is crucial to elucidate the mechanism underlying ovarian cancer tumorigenesis and progression and to define the determining events occurring during this process.

Elevated glycolysis is a hallmark of cancer cells (5, 6), and ovarian cancer is highly dependent on aerobic glycolysis to support cancer cell survival and therapeutic resistance (7). This elevated glycolytic activity is often linked to the activation of hypoxia-inducible factor 1 (HIF-1), a transcription factor that responds not only to hypoxic stress but also to various oncogenic, inflammatory, metabolic, and oxidative stressors (8–10). HIF-1 functions as a heterodimer composed of stable β subunits and unstable α subunits. Under normal oxygen conditions, the α subunits are rapidly degraded due to the sequential action of oxygen-dependent prolyl hydroxylases and the von Hippel–Lindau tumor suppressor (VHL) ubiquitin ligase (11–13). The activation of HIF-1α orchestrates mitochondrial metabolic reprogramming from oxidative phosphorylation (OXPHOS) to glycolysis by multiple mechanisms (8, 14, 15). Carbonic anhydrase 9 (*CA9*), a downstream target gene of HIF-1α, serves as a surrogate marker of hypoxia and actively promotes tumor glycolysis (16–18). Although the HIF-1α-CA9 axis has been reported to lead to elevated glycolysis and therapeutic resistance, there is no available therapeutic strategy to target this axis in ovarian cancer.

The ubiquitin–proteasome system (UPS), a fundamental "refuse processing plant" in eukaryotes, is responsible for the degradation of over 80% of cellular proteins (19). Ubiquitin, a small protein composed of 76 amino acids, has eight sites (M1, K6, K11,

Significance

Ovarian cancer is one of the most common cancers and the deadliest gynecologic cancer globally, yet the molecular mechanism underlying ovarian cancer initiation and development remains unclear. Here, we show that DNA methylation–mediated epigenetic silence of deubiquitinase Otubain 2 (*OTUB2*) enhances ubiquitination and degradation of its substrate sorting nexin 29 pseudogene 2 (SNX29P2). SNX29P2 functions as a linker protein that promotes the E3 ligase von Hippel–Lindau tumor suppressor-mediated degradation of hypoxia-inducible factor-1 alpha (HIF-1α). OTUB2 silencing increases the HIF-1α protein level and drives ovarian cancer initiation and chemoresistance via activation of its downstream target carbonic anhydrase 9 (*CA9*). Remarkably, inhibition of CA9 exhibits promising efficacy in suppressing ovarian cancer models with silenced OTUB2, either alone or in combination with conventional chemotherapy.

Author contributions: Y.N., X.W., Q.L., W.C., and Z.L. designed research; Y.N., X.W., Q.L., W.C., and P.Z. performed research; L.Z. contributed new reagents/analytic tools; Y.N., X.W., Q.L., and W.C. analyzed data; and Y.N., X.W., Q.L., and Z.L. wrote the paper.

The authors declare no competing interest.

This article is a PNAS Direct Submission.

[1]Y.N., X.W., Q.L., and W.C. contributed equally to this work.

[2]To whom correspondence may be addressed. Email: liuzh@cicams.ac.cn.

This article contains supporting information online at https://www.pnas.org/lookup/suppl/doi:10.1073/pnas.2315348121/-/DCSupplemental.

Published May 3, 2024.

K27, K29, K33, K48, and K63) that can be conjugated to another ubiquitin molecule, generating the ubiquitin code (20). The different types of polyubiquitin linkages determine the fate of substrates. For example, proteins modified by K48-linked ubiquitin chains are typically recognized and degraded by the 26S proteasome (21). Like other posttranslational modifications, ubiquitination can be reversed by deubiquitinases (DUBs). Ubiquitination and deubiquitination are broadly involved in regulating nearly every cellular process. Recently, emerging studies have revealed the important roles of DUBs in cancer development. DUBs regulate the stability, activity, or localization of important tumor suppressor proteins or oncoproteins and are thus potential targets for cancer treatment (22, 23). However, the landscape is complicated by the observation that some DUBs exert opposite effects in different contexts (24–30). Moreover, the upstream regulatory mechanisms of DUBs have not been fully elucidated.

In the present study, we aimed to systemically investigate the roles of DUBs in ovarian cancer development. We focused on DNA hypermethylation-induced suppression of DUBs, as epigenetic silencing is one of the most important nonmutational mechanisms that leads to the inactivation of tumor suppressors and cancer development. Through an unbiased screen of 45 DUBs, we identified Otubain 2 (*OTUB2*) as the DUB most suppressed by DNA methylation in ovarian cancer cells. Functional experiments using both transgenic mouse models and human cancer–derived models confirmed the critical tumor-suppressive role of OTUB2 in ovarian cancer. Intriguingly, we identified sorting nexin 29 pseudogene 2 (SNX29P2), an ill-defined protein with biased expression in ovarian tissue, as a bona fide substrate of OTUB2. The deubiquitination and stabilization of SNX29P2 by OTUB2 promotes the interaction between the E3 ligase VHL and HIF-1α and results in HIF-1α degradation, consequently inhibiting the expression of CA9. Activation of CA9 restores OTUB2-mediated inhibition of glycolysis and tumor growth; thus, CA9 inhibitors might be a promising strategy for ovarian cancer treatment.

Results

Silencing of *OTUB2* by DNA Hypermethylation Is Associated with Poor Prognosis in Ovarian Cancer Patients. To systematically investigate DUBs that are epigenetically silenced in ovarian cancer, we performed an unbiased screen by treating the ovarian cancer cell line ES-2 with the DNA methyltransferase inhibitor 5-azacytidine (5-aza) and detecting changes in the mRNA expression levels of 45 DUBs that belong to five different DUB families: ubiquitin carboxy-terminal hydrolases, Machado–Josephin domain–containing proteases, OTUs (ovarian tumor proteases), motif-interacting with ubiquitin-containing novel DUB family, and JAB1/MPN/MOV34 family (22). USPs (ubiquitin-specific proteases) family members were excluded from our screen because their roles in cancer have been well explored in recent years (31). Among the DUBs tested, *OTUB2* exhibited the most significant elevation in mRNA expression after treatment with 5-aza (Fig. 1*A*). Western blot analysis revealed that treatment with 5-aza significantly increased the protein level of OTUB2 in the ES-2 cells (Fig. 1*B*). We then evaluated OTUB2 protein expression and promoter methylation levels in a panel of ovarian cancer cell lines. All the four ovarian cancer cell lines with low OTUB2 expression (OVCA433, ES-2, 3AO, and A2780) showed high promoter methylation in the OTUB2 promoter region (Fig. 1 *C* and *D*). On the other hand, four out of the five cell lines with relatively high OTUB2 expression (SK-OV-3, OVTOKO, OVCA429, and OVCAR-3) exhibited either no or partial promoter methylation (Fig. 1 *C* and *D*). Additionally, compared to normal ovarian tissues, the majority of tumor tissues from ovarian cancer patients showed hypermethylation at the *OTUB2* promoter (Fig. 1*D*). These results suggested that the promoter methylation level of *OTUB2* is the principal regulator of OTUB2 expression. This conclusion was further confirmed by bisulfite genomic sequencing (BGS) (Fig. 1*E*). Moreover, treatment of 3AO and ES-2 cells, which have relatively low OTUB2 expression, with 5-aza substantially reduced the methylation level of the *OTUB2* promoter region (Fig. 1*F*).

Subsequently, to determine the relevance of *OTUB2* silencing to clinical features, we performed immunohistochemical (IHC) staining for OTUB2 in 150 ovarian cancer patient tissues (32). Kaplan–Meier analysis demonstrated that low OTUB2 expression was associated with poor overall survival and progression-free survival in ovarian cancer patients (Fig. 1 *G* and *H*). Furthermore, analysis of clinical variables showed that low OTUB2 expression was associated with ovarian cancer recurrence upon platinum treatment, indicating a potential role for OTUB2 in chemosensitivity (*SI Appendix*, Fig. S1*A*). In support of our data, analyses of data from The Cancer Genome Atlas (TCGA) public database also showed that low *OTUB2* expression was correlated with poor overall survival and progression-free survival in ovarian cancer (Fig. 1 *I* and *J*). In comparison, low *OTUB2* expression was correlated with favorable relapse-free survival in breast cancer (*SI Appendix*, Fig. S1*B*), and OTUB2 has been shown to be an oncoprotein that promotes breast cancer metastasis (33). Taken together, these data elucidate a potential tumor suppressor role for OTUB2 in ovarian cancer.

***OTUB2* Silencing Promotes Ovarian Cancer Progression.** To confirm the tumor-suppressive roles of OTUB2 in ovarian cancer development, we first generated an *Otub2*-knockout mouse model (34) (Fig. 2*A* and *SI Appendix*, Fig. S2*A*) and treated mice with wild-type *Otub2* ($Otub2^{wt/wt}$), heterozygous *Otub2* deletion ($Otub2^{wt/fl}$), and homozygous *Otub2* deletion ($Otub2^{fl/fl}$) with the carcinogen 7,12-dimethylbenz[a]anthracene (DMBA) (35, 36) to induce spontaneous cancer development (Fig. 2*B*). At 32 wk of age, the mice were killed to assess tumor incidence in various organs. Compared to that in the $Otub2^{wt/wt}$ group, the number of tumors in the liver, uterus, and ovary but not in other organs was dramatically greater in both the $Otub2^{fl/fl}$ group and $Otub2^{wt/fl}$ group (Fig. 2*C* and *SI Appendix*, Fig. S2*B*). No consistent increase in tumorigenesis was observed in the $Otub2^{fl/fl}$ group compared with the $Otub2^{wt/fl}$ group (Fig. 2*C*). These results indicated that *Otub2* is a haploinsufficient tumor suppressor gene in specific mouse organs, including the ovary, consistent with our hypothesis that the incomplete loss of *OTUB2* expression by DNA hypermethylation can promote ovarian cancer development in humans. To further investigate the tumor-suppressive function of OTUB2 in humans, we performed a limiting dilution assay using ES-2 cells expressing either an empty vector (EV) or OTUB2. Compared to control cells, OTUB2-expressing ES-2 cells exhibited significantly delayed tumor formation (Fig. 2*D* and *SI Appendix*, Fig. S2*C*). Consistent with these findings, in the OVCA429 cell line, which exhibits high OTUB2 expression, we observed markedly increased tumorigenic potential after OTUB2 depletion (Fig. 2*E* and *SI Appendix*, Fig. S2*D*).

We next determined whether OTUB2 affects other characteristics during ovarian cancer progression. Overexpression of OTUB2 in ES-2 and A2780 cells significantly reduced cell proliferation (Fig. 2*F* and *SI Appendix*, Fig. S2 *E* and *G*). OTUB2 depletion by two independent shRNAs promoted the proliferation of OVCA429 cells (Fig. 2*G* and *SI Appendix*, Fig. S2 *F* and *H*). In addition, OTUB2-overexpressing ovarian cancer cells showed

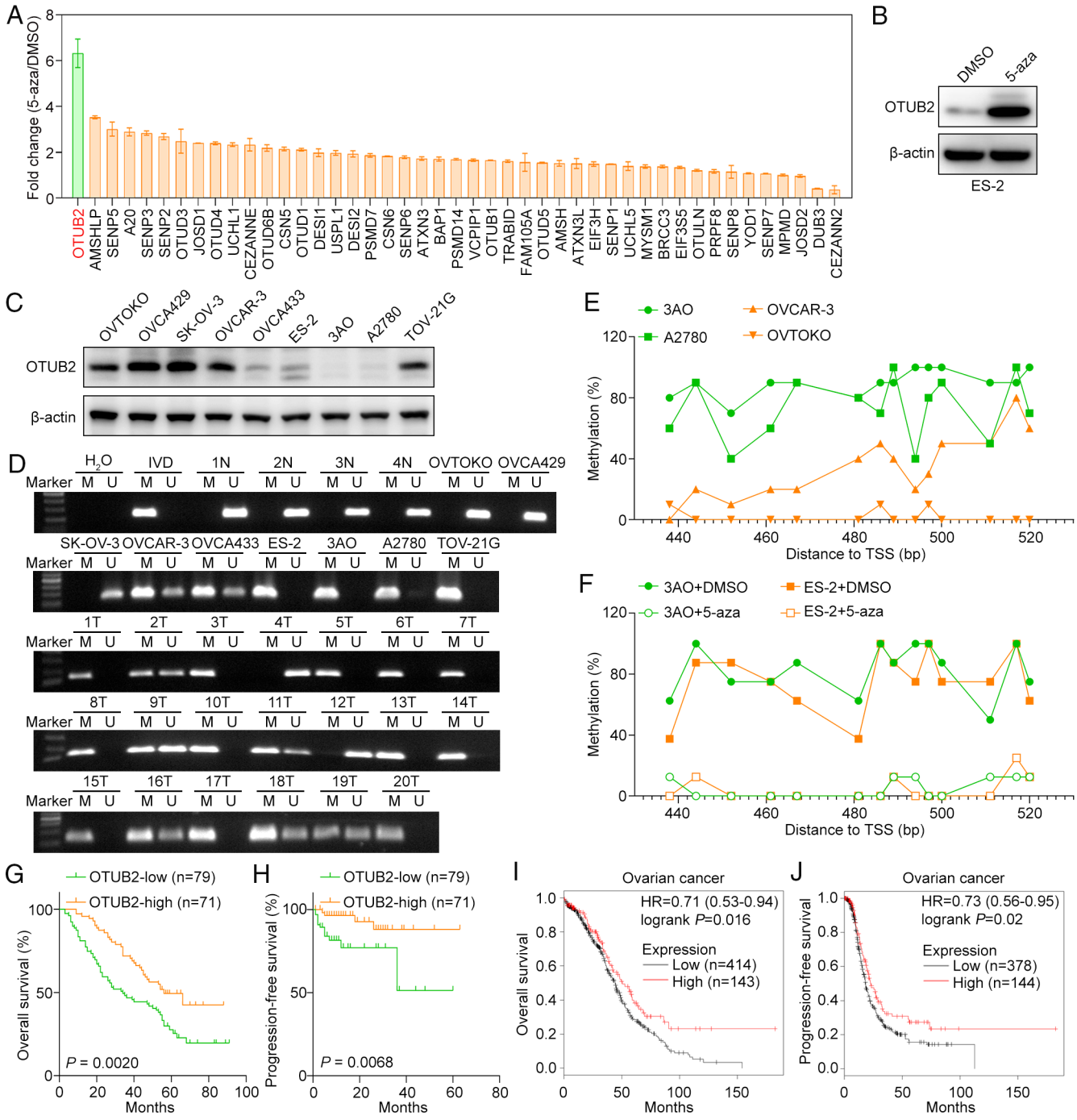

Fig. 1. Silencing of OTUB2 by DNA hypermethylation is correlated with poor prognosis in ovarian cancer patients. (*A*) Relative gene expression levels of 45 DUBs in cells treated with 5-aza (10 μM) compared to those in cells treated with DMSO. (*B*) Western blot analysis of OTUB2 protein expression in cells treated with 5-aza (10 μM) compared to that in cells treated with DMSO. (*C*) Western blot analysis of OTUB2 expression levels in a panel of ovarian cancer cell lines. (*D*) Methylation-specific PCR was performed to evaluate OTUB2 promoter methylation levels in ovarian cancer cell lines and patient samples. (*E* and *F*) BGS was used to evaluate the methylation levels of the OTUB2 promoter region in various ovarian cancer cell lines (*E*) and in ovarian cancer cell lines treated with 5-aza or DMSO (*F*). Methylation percentages were calculated from the number of methylated clones among the 10 clones picked for sequencing. (*G* and *H*) Prognostic analyses of ovarian cancer patients with low or high OTUB2 expression (stratified by the mean OTUB2 expression level in all samples). Kaplan–Meier survival plots are shown. (*I* and *J*) Prognoses of ovarian cancer patients with low or high OTUB2 expression from the TCGA database.

increased apoptosis and sensitivity to carboplatin (CBP), while OTUB2-silenced cells developed chemoresistance (Fig. 2 *H–K* and *SI Appendix*, Fig. S2 *I–L*). The roles of OTUB2 in suppressing ovarian cancer growth and chemoresistance were further supported by in vivo xenograft assays (Fig. 2 *L* and *M*). Importantly, we did not observe similar effects after overexpression of an enzymatically inactivated OTUB2^{C51S} mutant (in which cysteine 51 was replaced with serine) in any of the above assays (Fig. 2 *F*, *H*, *J*, *L*, and *M* and *SI Appendix*, Fig. S2 *E*, *G*, *I*, and *K*), indicating that the tumor-suppressive effect of OTUB2 was dependent on its enzymatic activity.

OTUB2 Deubiquitinates and Stabilizes SNX29P2. To delineate the mechanism underlying the tumor-suppressive role of OTUB2 in ovarian cancer, tumors derived from EV-, OTUB2^{wt}-, or OTUB2^{C51S}-expressing ES-2 cells (Fig. 2*L*) were subjected to proteomic analysis. Consistent with the finding that the tumor-suppressive functions of OTUB2 are dependent on its enzymatic

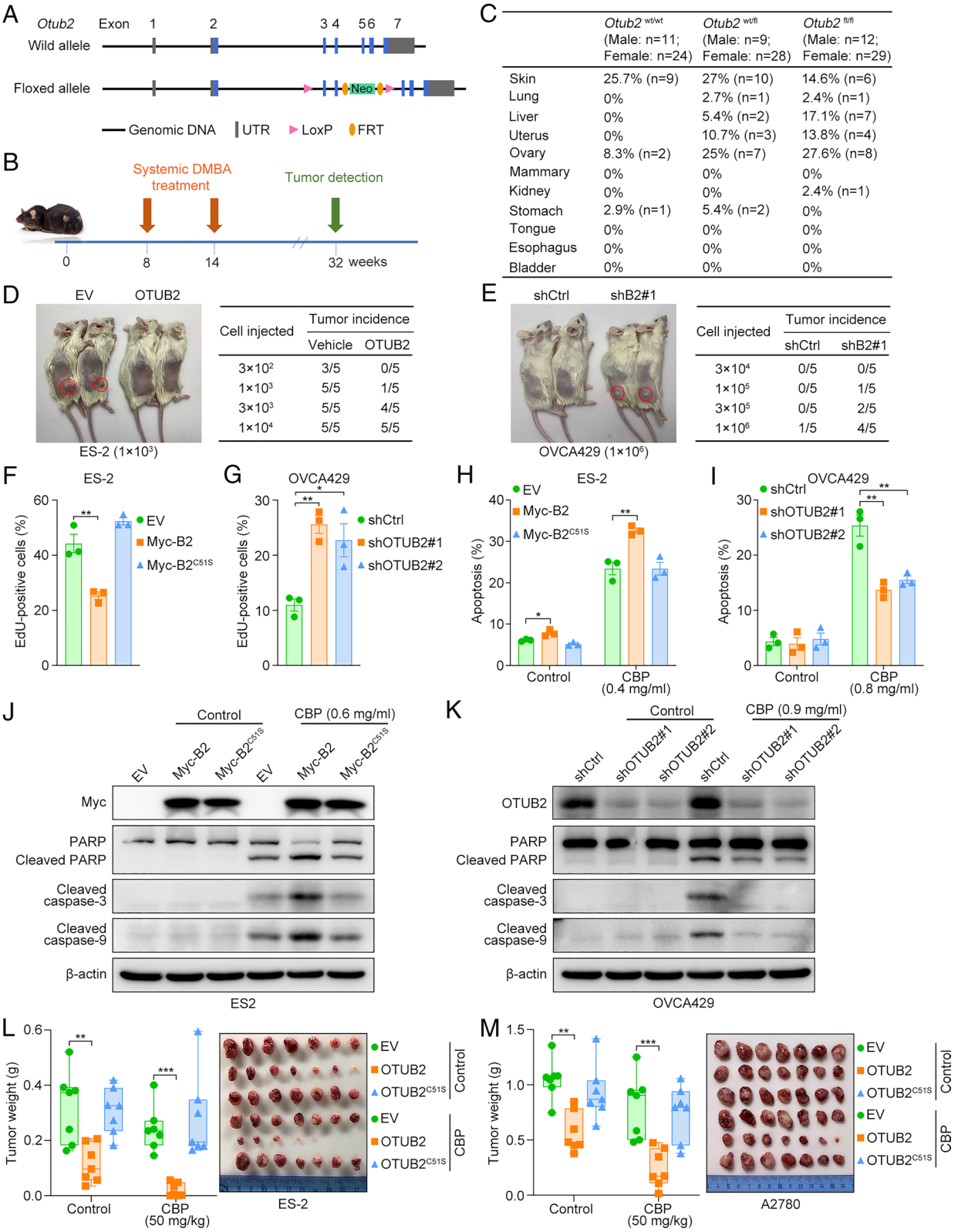

Fig. 2. OTUB2 silencing promotes ovarian cancer progression. (*A* and *B*) Schematics showing the *Otub2*-knockout strategy for the mouse model (*A*) and the DMBA induction experimental timeline (*B*). (*C*) Tumor incidence in various organs from 32-wk-old *Otub2*$^{wt/wt}$, *Otub2*$^{wt/fl}$, and *Otub2*$^{fl/fl}$ mice. (*D* and *E*) Representative images and tumor incidence in limiting dilution assays with control and OTUB2-overexpressing ES-2 cells (*D*) and with control and OTUB2-knockdown OVCA429 cells (*E*). (*F* and *G*) Statistical analyses of the percentage of EdU-positive cells in the indicated cells. The percentage of EdU-positive cells was calculated from the number of positive cells among the 20 total cells examined. Triplicate data were collected from three random fields of view of each group. The data are presented as the mean ± SD values; unpaired Student's *t* test, **P* < 0.05, ***P* < 0.01; n = 3. (*H* and *I*) Apoptosis rates of the indicated cells treated with CBP at the indicated concentrations for 24 h. The data are presented as the mean ± SD values; unpaired Student's *t* test, **P* < 0.05, ***P* < 0.01; n = 3. (*J* and *K*) Western blot analysis of apoptosis markers in the indicated cells. Cells were treated with CBP at the indicated concentrations for 24 h before analysis. (*L* and *M*) Representative images and weights of xenografts generated with the indicated cell lines. Box plot representation: from *Top* to *Bottom*—maximum, 75th percentile, median, 25th percentile, and minimum values; unpaired Student's *t* test, ***P* < 0.01, ****P* < 0.001; n = 7.

activity, a total of 59 proteins were consistently up-regulated in OTUB2^{wt}-expressing cells compared to both EV- and OTUB2^{C51S}-expressing cells, while only 15 were consistently up-regulated in OTUB2^{wt}- and OTUB2^{C51S}-expressing cells compared with EV-expressing cells (Fig. 3*A*). Among the 55 proteins whose expression was consistently up-regulated in the OTUB2^{wt} group compared to that in the other two groups but not in the OTUB2^{C51S} group compared to that in the control group, we focused on SNX29P2 for further validation, as it exhibited the highest fold change, and its biased high expression in the ovary suggested a potential tumor-suppressive role (*SI Appendix*, Fig. S3*A*). Since *SNX29P2* is defined as a pseudogene in several public databases, we first confirmed the protein-coding ability of *SNX29P2* by expressing Flag-tagged SNX29P2 in 293T cells (*SI Appendix*, Fig. S3*B*). We subsequently determined whether OTUB2 affects SNX29P2 protein stability. No anti-SNX29P2 antibody was commercially available, and we failed to generate a custom-made antibody. Thus, we utilized ovarian cancer cell lines stably expressing Flag-tagged SNX29P2 as models for subsequent studies. The results of cycloheximide (CHX) pulse–chase assays showed that the half-life of the SNX29P2 protein was prolonged in A2780 and ES-2 cells overexpressing OTUB2^{wt} but not in those overexpressing OTUB2^{C51S} (Fig. 3 *B* and *C*). Additionally, OTUB2-knockdown in ES-2 cells reduced the protein stability of SNX29P2 (Fig. 3*D*). In contrast, the mRNA level of SNX29P2 was not affected by either OTUB2 overexpression or OTUB2-knockdown in ovarian cancer cells (*SI Appendix*, Fig. S3 *C* and *D*).

To confirm whether OTUB2 functions as a bona fide DUB of SNX29P2, we first demonstrated that both OTUB2 and SNX29P2 were localized predominantly in the nucleus in ovarian cancer cells (Fig. 3*E*). Next, the direct interaction between these two proteins was confirmed by in vivo and in vitro coimmunoprecipitation (co-IP) assays (Fig. 3 *F* and *G*). The interaction between OTUB2 and SNX29P2 was diminished after enzymatic inactivation of OTUB2 (Fig. 3*H*), further supporting the conclusion that OTUB2 exerts its enzymatic activity–dependent tumor-suppressive function through an interaction with SNX29P2. The same conclusions were obtained from a proximity ligation assay (PLA) in ES-2 and A2780 cells stably expressing Myc-OTUB2 and Flag-SNX29P2 (Fig. 3*I*). Finally, the direct deubiquitination of SNX29P2 by OTUB2 was validated by an in vitro deubiquitination assay (Fig. 3*J*). Western blot analysis of different ubiquitin linkage types indicated that OTUB2 cleaves mainly K48-linked polyubiquitin chains, a well-studied ubiquitin linkage type that contributes to the degradation of proteins (20), on SNX29P2 (*SI Appendix*, Fig. S3 *E* and *F*). Taken together, the above results indicate that OTUB2 stabilizes the SNX29P2 protein via deubiquitination.

OTUB2/SNX29P2 Suppresses Glycolysis and Promotes OXPHOS in Ovarian Cancer. To investigate the downstream pathways regulated by OTUB2/SNX29P2, we performed RNA sequencing (RNA-seq) in ES-2 cells expressing EV, OTUB2, or SNX29P2. The results of gene set enrichment analysis (GSEA) indicated that overexpression of either OTUB2 or SNX29P2 suppresses the glycolysis pathway and enhances OXPHOS activity (Fig. 4 *A* and *B*). To further validate these results, we performed Seahorse assays to directly evaluate the effects of OTUB2 and SNX29P2 on glycolysis and OXPHOS. Overexpression of OTUB2 or SNX29P2 in ES-2 cells inhibited glycolysis and lactate production while increasing OXPHOS (Fig. 4 *C*–*E* and *SI Appendix*, Fig. S4 *A*–*C*). However, overexpression of the inactivated OTUB2^{C51S} mutant did not affect glycolysis or OXPHOS (Fig. 4 *C*–*E* and *SI Appendix*, Fig. S4 *A*–*C*). Next, we quantified glycolysis and OXPHOS activity in control and OTUB2-silenced OVCA429 cells (*SI Appendix*, Fig. S4*D*). The results indicated that silencing OTUB2 significantly increased glycolytic capacity and lactate production and inhibited OXPHOS (Fig. 4 *F*–*H* and *SI Appendix*, Fig. S4 *E* and *F*). Furthermore, the increased glycolysis and decreased OXPHOS mediated by OTUB2 silencing could be effectively reversed by the expression of shRNA-resistant wild-type OTUB2 (*SI Appendix*, Fig. S4 *G*–*L*). In contrast, ectopic expression of shRNA-resistant OTUB2^{C51S} mutant failed to rescue the observed phenotypes (*SI Appendix*, Fig. S4 *G*–*L*). Subsequently, silencing of SNX29P2 phenocopied the effects of OTUB2 depletion on cell metabolism (Fig. 4 *I*–*K* and *SI Appendix*, Fig. S4 *M*–*O*). Moreover, overexpression of SNX29P2 in OTUB2-silenced OVCA429 cells abrogated the increases in glycolysis and the lactate level mediated by OTUB2-knockdown (Fig. 4 *L* and *M* and *SI Appendix*, Fig. S4 *P* and *Q*). The decrease in OXPHOS mediated by OTUB2-knockdown was also rescued by overexpression of SNX29P2 (Fig. 4*N* and *SI Appendix*, Fig. S4*R*). These results indicate that OTUB2 stabilizes SNX29P2 to reprogram ovarian cancer cell metabolism, facilitating a shift from a glycolysis-dominant phenotype to an OXPHOS-dominant phenotype.

SNX29P2 Promotes VHL-Mediated HIF-1α Degradation to Inhibit Downstream *CA9* Transcription. Having demonstrated that OTUB2/SNX29P2 causes impaired glycolysis and increased OXPHOS in ovarian cancer cells, we then identified the mediator of this function. We analyzed the RNA-seq data and found that a total of 75 genes were consistently down-regulated in both OTUB2-overexpressing cells and SNX29P2-overexpressing cells (Fig. 5*A*). Among these genes, CA9, a well-known transcriptional target of HIF-1α that facilitates glycolysis in cancer (16–18), was the most markedly down-regulated gene (Fig. 5*A*). Accordingly, GSEA indicated that OTUB2 and SNX29P2 were significantly negatively correlated with hypoxia in ovarian cancer cells (Fig. 5*B*). Therefore, we investigated whether OTUB2/SNX29P2 inhibits *CA9* transcriptional activation mediated by HIF-1α. Western blotting indicated that overexpression of OTUB2 and SNX29P2 reduced the protein expression levels of HIF-1α and CA9 under normoxic conditions, whereas the inactivated OTUB2^{C51S} mutant did not exert such effects (Fig. 5*C*). Additionally, under hypoxic conditions, the expression of HIF-1α and CA9 was significantly increased, and the decreases in HIF-1α and CA9 protein expression levels mediated by overexpression of OTUB2 and SNX29P2 were abolished (Fig. 5*C*). Furthermore, the RT–qPCR results confirmed the modulation of *CA9* mRNA expression by both OTUB2 and SNX29P2 (*SI Appendix*, Fig. S5*A*). Subsequently, we sought to determine whether SNX29P2 mediates the modulatory effect of OTUB2 on HIF-1α and CA9 expression. As expected, overexpression of SNX29P2 inhibited the increases in the expression of HIF-1α and CA9 mediated by OTUB2 silencing under normoxic conditions, but these effects were abrogated under hypoxic conditions (Fig. 5*D* and *SI Appendix*, Fig. S5*B*).

Given that both OTUB2 and SNX29P2 reduced the protein expression level of HIF-1α but did not affect its mRNA level (*SI Appendix*, Fig. S5*C*), we investigated whether OTUB2 and SNX29P2 regulate the posttranslational modification of HIF-1α. We first treated control, OTUB2-overexpressing, and SNX29P2-overexpressing ES-2 cells with the proteasome inhibitor MG132 and found that OTUB2/SNX29P2-mediated HIF-1α protein degradation was reestablished by MG132 treatment (*SI Appendix*, Fig. S5*D*). In comparison, inhibition of the autophagy–lysosome pathway with the lysosome inhibitor ammonium chloride or the autophagosome inhibitor 3-methyladenine did not affect OTUB2/SNX29P2-mediated HIF-1α degradation (*SI Appendix*, Fig. S5*D*). Subsequently, CHX pulse–chase assays showed that overexpression

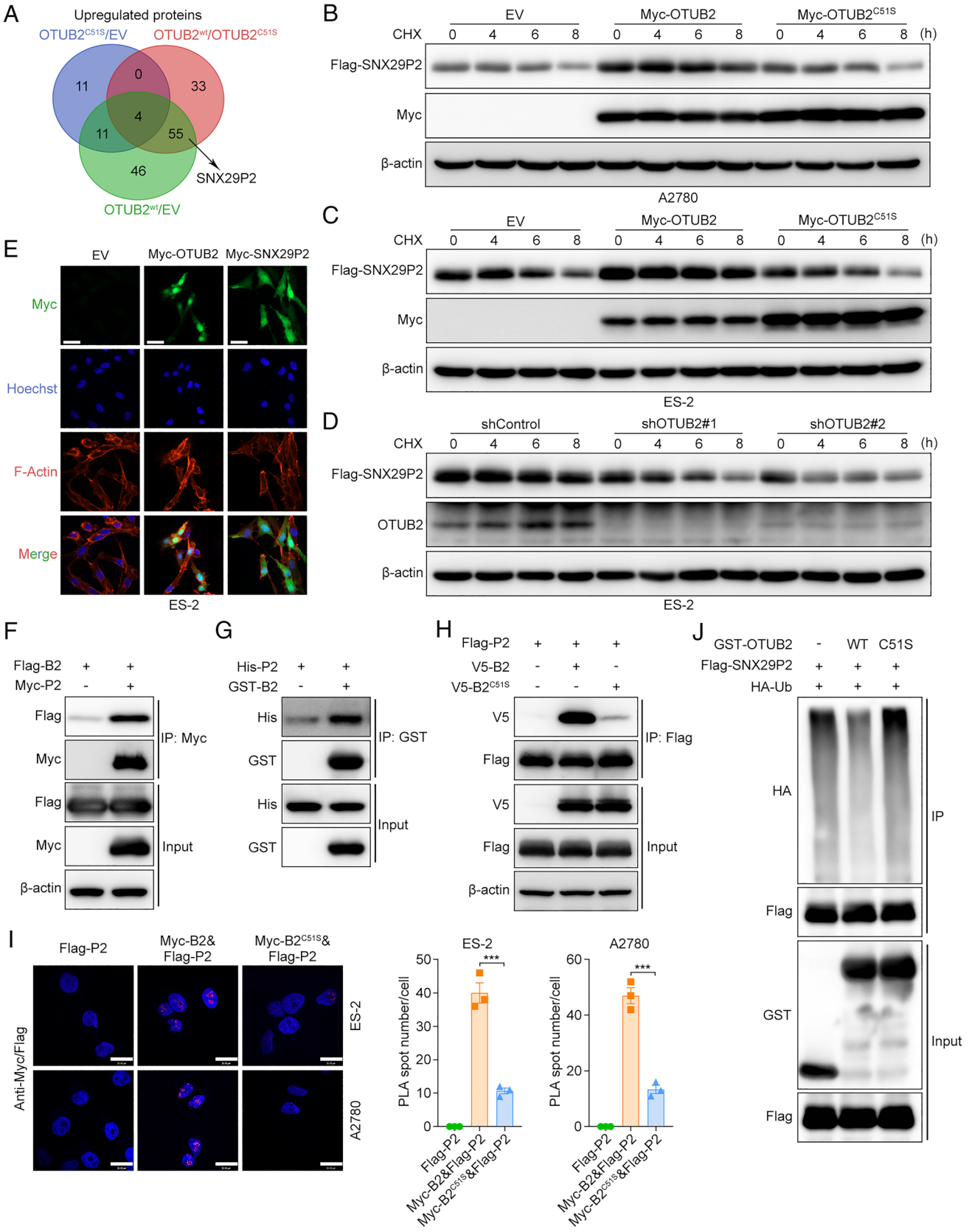

Fig. 3. OTUB2 deubiquitinates and stabilizes SNX29P2. (*A*) Number of significantly differentially expressed proteins identified by proteomic analyses of the indicated groups. (*B–D*) Western blot analysis of the indicated proteins in the CHX pulse–chase assay. (*E*) IF assay showing the predominant subcellular localization of Myc-OTUB2 and Myc-SNX29P2 in the nucleus. (*F–H*) Western blot analysis of the indicated proteins in vivo (*F* and *H*) and in vitro (*G*) co-IP assays. (*I*) Representative images of the merged PLA signals and quantitative analysis of PLA puncta in the indicated cells. The scale bar represents 30 μm. The data are presented as the mean ± SEM. values; unpaired Student's *t* test, ***$P < 0.001$; n = 3. (*J*) Western blot analysis of the indicated proteins in the in vitro deubiquitination assay.

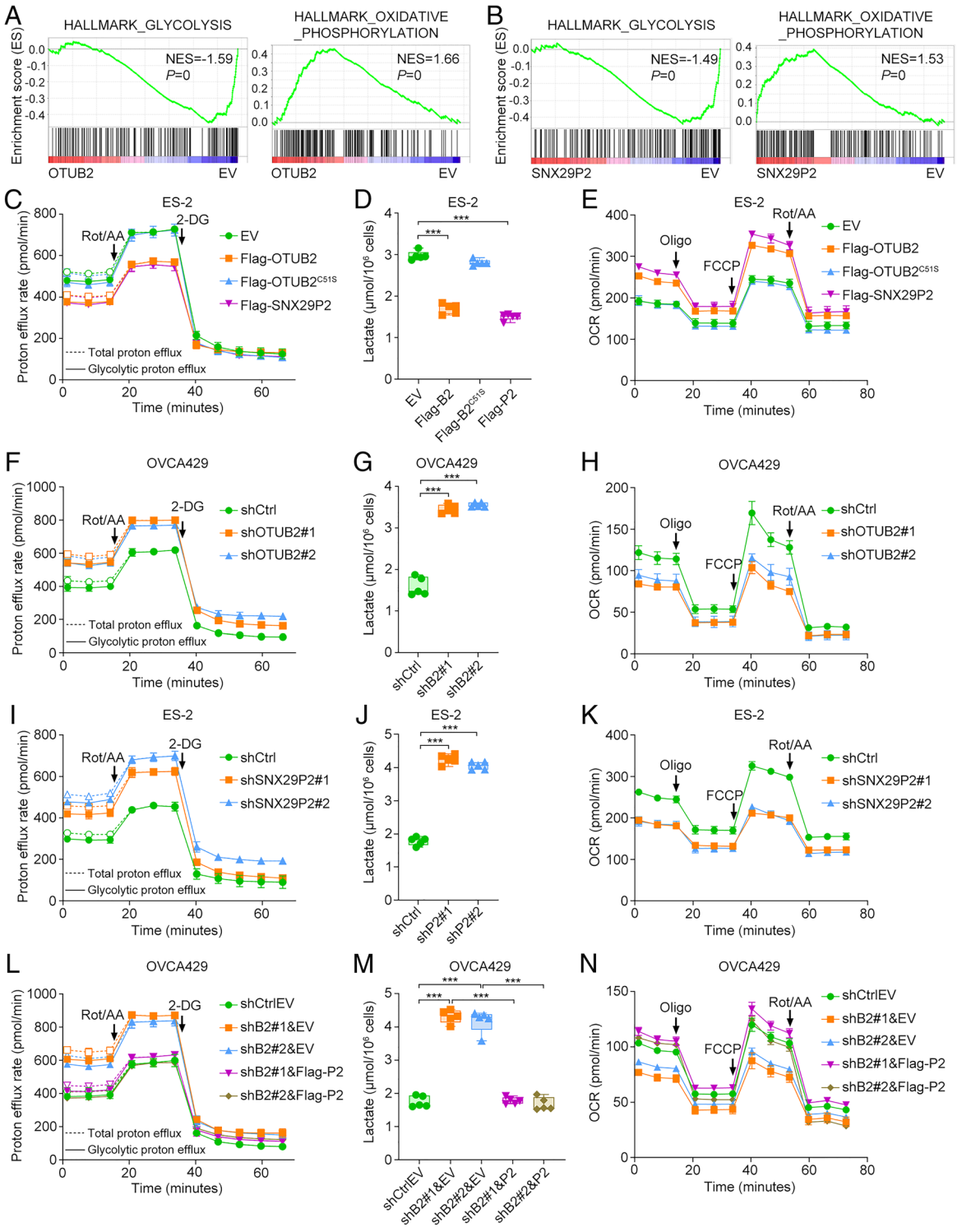

Fig. 4. OTUB2/SNX29P2 suppresses glycolysis and increases OXPHOS in ovarian cancer. (*A* and *B*) Enriched pathways identified by GSEA based on RNA-seq data from ES-2 cells expressing EV, OTUB2, or SNX29P2. (*C*) Measurement of glycolytic capacity using a Seahorse assay in EV-, OTUB2-, or SNX29P2-expressing ES-2 cells. The data are presented as the mean ± SD values; n = 3. (*D*) Measurement of lactate production in EV-, OTUB2-, or SNX29P2-expressing ES-2 cells. Box plot representation: from *Top* to *Bottom*—maximum, 75th percentile, median, 25th percentile, and minimum values; unpaired Student's *t* test, ***$P < 0.001$; n = 5. (*E*) Measurement of the OCR using a Seahorse assay in EV-, OTUB2-, or SNX29P2-expressing ES-2 cells. The data are presented as the mean ± SD values; n = 3. (*F*) Measurement of glycolytic capacity using a Seahorse assay in control and OTUB2-silenced OVCA429 cells. The data are presented as the mean ± SD values; n = 3. (*G*) Measurement of lactate production in control and OTUB2-silenced OVCA429 cells. Box plot representation: from *Top* to *Bottom*—maximum, 75th percentile, median, 25th percentile, and minimum values; unpaired Student's *t* test, ***$P < 0.001$; n = 5. (*H*) Measurement of the OCR using a Seahorse assay in control and OTUB2-silenced OVCA429 cells. The data are presented as the mean ± SD values; n = 3. (*I*) Measurement of the glycolytic capacity using a Seahorse assay in control and SNX29P2-silenced ES-2 cells. The data are presented as the mean ± SD values; n = 3. (*J*) Measurement of lactate production in control and SNX29P2-silenced ES-2 cells. Box plot representation: from *Top* to *Bottom*—maximum, 75th percentile, median, 25th percentile, and minimum values; unpaired Student's *t* test, ***$P < 0.001$; n = 5. (*K*) Measurement of the OCR using a Seahorse assay in control and SNX29P2-silenced ES-2 cells. The data are presented as the mean ± SD values; n = 3. (*L*) Measurement of the glycolytic capacity using a Seahorse assay in the indicated cells. The data are presented as the mean ± SD values; n = 3. (*M*) Measurement of lactate production in the indicated cells. Box plot representation: from *Top* to *Bottom*—maximum, 75th percentile, median, 25th percentile, and minimum values; unpaired Student's *t* test, ***$P < 0.001$; n = 5. (*N*) Measurement of the OCR using a Seahorse assay in the indicated cells. The data are presented as the mean ± SD values; n = 3.

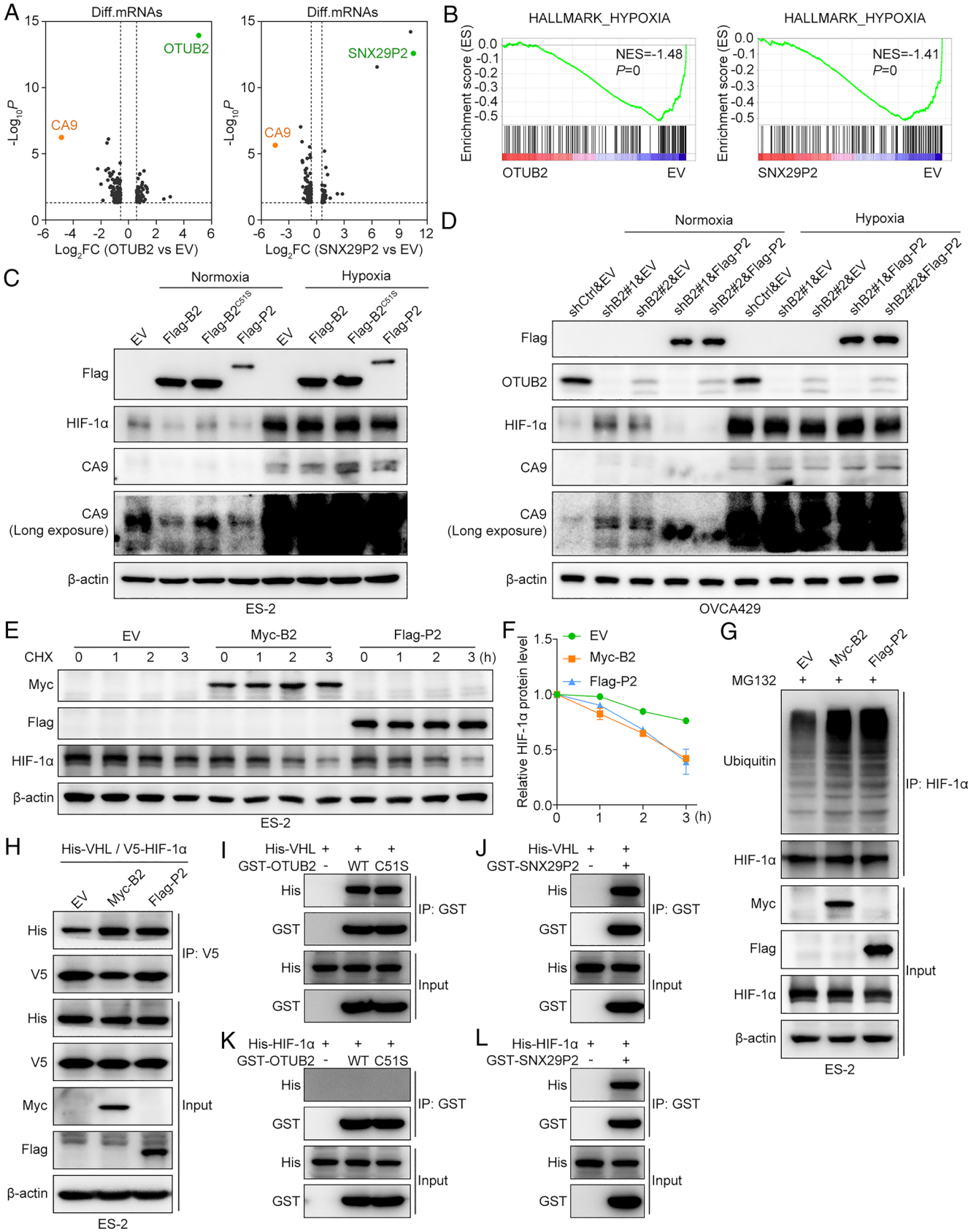

Fig. 5. SNX29P2 promotes VHL-mediated HIF-1α degradation to inhibit CA9 transcription. (*A*) Volcano plots showing up-regulated and down-regulated mRNAs in OTUB2- and SNX29P2-overexpressing ES-2 cells compared to control cells. (*B*) Enriched pathways identified by GSEA based on RNA-seq data from ES-2 cells expressing EV, OTUB2, or SNX29P2. (*C* and *D*) Western blot analysis of HIF-1α and CA9 expression in the indicated cells under normoxic and hypoxic conditions. (*E* and *F*) Western blot (*E*) and quantitative analyses (*F*) of HIF-1α protein expression in the CHX pulse–chase assay. (*G*) Western blot analysis to assess HIF-1α ubiquitination in the indicated cells. (*H*) Western blot analysis of the indicated proteins in the co-IP assays to detect the interaction between HIF-1α and VHL. (*I*–*L*) Western blot analysis for the indicated proteins in the in vitro co-IP assays.

of OTUB2 and SNX29P2 shortened the half-life of the endogenous HIF-1α protein (Fig. 5 *E* and *F*). Additionally, ubiquitination assays indicated that overexpression of OTUB2 and SNX29P2 increased the level of ubiquitinated HIF-1α (Fig. 5*G*). Next, we investigated the direct mechanism by which OTUB2/SNX29P2 promotes UPS-mediated HIF-1α degradation. Under normoxic conditions, the HIF-1α protein is recognized by VHL, an E3 ubiquitin ligase responsible for its degradation (11, 37). We sought to determine whether OTUB2/SNX29P2 modulates VHL-mediated HIF-1α degradation. Neither OTUB2 nor SNX29P2 affected the protein expression of VHL (*SI Appendix*, Fig. S5*E*). IP revealed that overexpression of both OTUB2 and SNX29P2 promoted the interaction between VHL and HIF-1α (Fig. 5*H*). Furthermore, in vitro co-IP assays demonstrated that both OTUB2 and SNX29P2 directly interact with VHL and that the interaction between OTUB2 and VHL is independent of the enzymatic activity of OTUB2 (Fig. 5 *I* and *J*). However, only SNX29P2, but not OTUB2, directly interacted with HIF-1α (Fig. 5 *K* and *L*). These results suggest that SNX29P2 promotes VHL-mediated HIF-1α degradation and subsequent *CA9* transcriptional repression. Finally, to investigate whether CA9 is involved in the regulation of OTUB2/SNX29P2 on cancer metabolism, we overexpressed CA9 in OTUB2- and SNX29P2-overexpressing ES-2 cells and then analyzed glycolysis and OXPHOS (*SI Appendix*, Fig. S5*F*). Overexpression of CA9 abolished the decreases in glycolysis and lactate production and the increase in OXPHOS caused by overexpression of OTUB2 and SNX29P2 (*SI Appendix*, Fig. S5 *G–K*). These findings highlight CA9 as a key regulator that mediates the functions of OTUB2 and SNX29P2 in ovarian cancer.

CA9 Is a Promising Target in OTUB2-Silenced Ovarian Cancer. Subsequently, to understand whether CA9 is the critical downstream target that mediates the tumor suppressive effects of OTUB2/SNX29P2 in ovarian cancer, we initially investigated the effect of genetically targeting *CA9* on ovarian cancer growth. Knockdown of CA9 in ES-2 and A2780 cells dramatically inhibited ovarian cancer cell proliferation, and ectopic overexpression of shRNA-resistant wild-type CA9 restored this effect, while the shRNA-resistant catalytically inactive mutants of CA9 (E238A and T33A) failed to restore decreased cell proliferation (*SI Appendix*, Fig. S6 *A* and *B*). Importantly, treatment with SLC-0111, a pharmacological inhibitor of CA9, significantly inhibited cell proliferation even in cells overexpressing wild-type CA9 (*SI Appendix*, Fig. S6*B*). Furthermore, the oncogenic roles of CA9 in ovarian cancer and the therapeutic potential of SLC-0111-mediated CA9 inhibition were confirmed in xenograft models from ES-2 cells (Fig. 6 *A* and *B*). These results indicate that CA9 promotes the progression of ovarian cancer in an enzymatically dependent manner, and targeting CA9 with SLC-0111 inhibits ovarian cancer progression. Next, to investigate the therapeutic potential of targeting CA9 in OTUB2-silenced ovarian cancer, we first tested the sensitivity of ovarian cancer cell lines to SLC-0111 during in vitro treatment. We found that treatment with SLC-0111 significantly enhanced chemosensitivity in ES-2 and A2780 cells with low OTUB2 expression but did not affect the sensitivity of OVCA492 cells with high OTUB2 expression to CBP (*SI Appendix*, Fig. S6*C*). Subsequently, we determined the therapeutic potential of the CA9 inhibitor in xenograft models established with ES-2 and A2780 cells. Treatment with SLC-0111 as a single agent significantly reduced the tumor burden and further synergized with CBP to achieve a combination index of 0.47 and 0.22 in ES-2 and A2780 xenografts, respectively (Fig. 6 *C–F*). In addition, we established three peritoneal carcinomatosis models derived from two OTUB2-silenced ovarian cancer cell lines (ES-2 and A2780) and one high OTUB2-expressed cell line (OVCA429) to validate the therapeutic efficacy of CA9 inhibition. The results indicated that in the both ES-2 and A2780 models with silenced OTUB2 expression, SLC-0111 treatment significantly increased the chemosensitivity to CBP, showing a robust synergistic therapeutic effect (Fig. 6 *G* and *H*). However, in the OVCA429 model with high OTUB2 expression, treatment with SLC-0111 had no impact on the sensitivity to CBP (Fig. 6 *G* and *H*). Taken together, these results demonstrate the unique vulnerability of OTUB2-silenced ovarian cancer to pharmacological inhibition of CA9.

Finally, to determine the clinical relevance of CA9 expression in ovarian cancer, we examined the CA9 protein levels in the same cohort described in Fig. 1 by IHC staining. Kaplan–Meier analysis showed that high expression of CA9 was correlated with poor survival in ovarian cancer patients (Fig. 6 *I* and *J*). Moreover, correlation analysis indicated that the expression of CA9 was negatively correlated with that of OTUB2 in ovarian cancer patients (*SI Appendix*, Fig. S6 *D* and *E*). Consistent with this result, the significant negative correlation between CA9 and OTUB2 protein levels was validated in a panel of ovarian cancer cell lines (Fig. 1*C* and *SI Appendix*, Fig. S6*F*). These findings further support the important roles of CA9 in ovarian cancer progression and the negative regulatory effect of OTUB2 on CA9 expression in ovarian cancer.

Discussion

Ubiquitination and deubiquitination play crucial roles in various biological events, and accumulating evidence suggests the importance of DUBs in cancer progression. However, although the roles and mechanisms of USP DUB family members have been well explored in recent years, the role of a large fraction of the other DUB families in human cancer has not been fully elucidated. Moreover, the functions of DUBs in human cancer appear to be highly context dependent, as the same DUB functions as either an oncoprotein or a tumor suppressor in different cancer types (24–30). Similarly, OTUB2 has been previously reported to function as an oncoprotein in several cancer types, including breast cancer (33), lung cancer (38), gastric cancer (39, 40), and colorectal cancer (41). However, our recent study demonstrated a tumor-suppressive role for OTUB2 in tongue and esophageal squamous cell carcinomas (34). In the current study, we identified ovarian cancer as another cancer type that can be driven by OTUB2 silencing. Interestingly, despite functioning as a tumor suppressor in both squamous cell carcinoma and ovarian cancer, OTUB2 acts through completely different mechanisms in these two contexts. In oral and esophageal squamous cell carcinomas, OTUB2 activates CALML3 (34), a specific marker of the squamous epithelium (42–44), to exert its tumor-suppressive effects. In contrast, in ovarian cancer, we found that SNX29P2 is the critical substrate of OTUB2, and SNX29P2 exhibits biased high expression in the ovary compared to other tissues (*SI Appendix,* Fig. S3*A*). These findings highlight the complex functional mechanism of DUBs in cancer and underscore the need for further research to elucidate this process.

Although *SNX29P2* was initially annotated as a pseudogene, it is annotated as a protein-coding gene in several databases (45, 46) and was identified in our study as the most significantly up-regulated protein upon ectopic OTUB2 expression. Our multiple in vivo and in vitro assays confirmed that SNX29P2 is the critical substrate of OTUB2 and mediates its tumor-suppressive functions of OTUB2 in ovarian cancer. Thus, our study delineated a role of SNX29P2 in cancer development, revealing its tumor-suppressive role in ovarian cancer. However, a major limitation of our study is the lack of

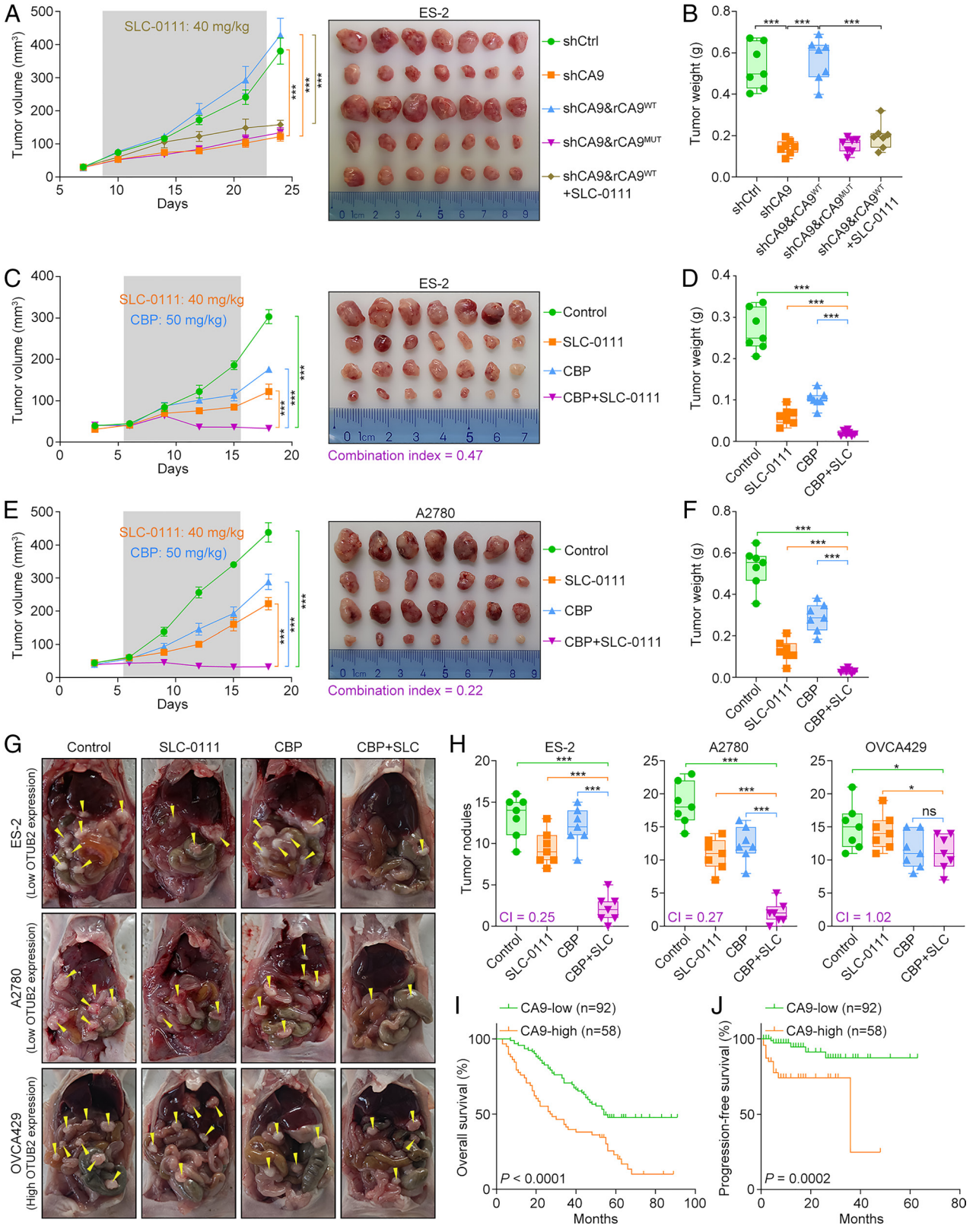

Fig. 6. CA9 is a promising target in OTUB2-silenced ovarian cancer. (*A* and *B*) Growth curves and representative images (*A*) and weights (*B*) of xenograft tumors generated from the indicated cells. SLC-0111 was administered at a concentration of 40 mg/kg every 2 d. The data are presented as the mean ± SEM values in *A*. Box plot representation: from *Top* to *Bottom*—maximum, 75th percentile, median, 25th percentile, and minimum values in (*B*); unpaired Student's *t* test, ***$P < 0.001$; n = 7. (*C*–*F*) Growth curves and representative images (*C* and *E*) and weights (*D* and *F*) of the xenograft tumors from ES-2 and A2780 cells. The data are presented as the mean ± SEM values in (*C* and *E*). Box plot representation: from *Top* to *Bottom*—maximum, 75th percentile, median, 25th percentile, and minimum values in (*D* and *F*); unpaired Student's *t* test, ***$P < 0.001$; n = 7. (*G* and *H*) Representative images and quantitative analysis of metastatic nodules in the abdomens of mice injected with OTUB2-silenced cells (ES-2 and A2780) and OTUB2-expressing cells (OVCA429). Box plot representation: from *Top* to *Bottom*—maximum, 75th percentile, median, 25th percentile, and minimum values; unpaired Student's *t* test, *$P < 0.05$, ***$P < 0.001$, ns: no significance; n = 7. (*I* and *J*) Prognostic analyses of ovarian cancer patients with low or high CA9 expression (stratified by the mean CA9 expression level in all samples). Kaplan–Meier survival plots are shown.

SNX29P2-specific antibodies, and our attempt to produce an in-house antibody was unsuccessful. Although our conclusions using multiple experimental models are convincing, the development of SNX29P2-specific antibodies is still necessary for future studies.

Cancer metabolic reprogramming has been well established since the discovery of the Warburg effect (47–49). The phenomenon of increased aerobic glycolysis is now widely recognized as a hallmark of numerous cancers and has become a crucial target for cancer therapy as well as a diagnostic biomarker (50). CA9 is considered a transcriptional target of HIF-1α and surrogate marker of tumor hypoxia and is widely regarded as a prominent biomarker of poor patient prognosis in many solid tumors (17, 51–53). The safety of the CA9 inhibitor SLC-0111 in clinical treatment was also evaluated in a recent clinical trial (54). Our study revealed that CA9 acts as a key mediator of metabolic remodeling to facilitate glycolysis in ovarian cancer. OTUB2/SNX29P2 act as upstream regulators of CA9, mediating the transcriptional suppression of *CA9* by triggering VHL-mediated HIF-1α degradation, eventually suppressing cancer glycolysis and development. Importantly, our findings suggest the unique vulnerability of OTUB2-silenced ovarian cancer to pharmacological inhibition of CA9, which provides the rationale for subsequent clinical trials testing CA9 inhibitors in ovarian cancer treatment (*SI Appendix*, Fig. S6*G*).

Materials and Methods

Ovarian cancer samples were collected from 150 patients with ovarian serous adenocarcinoma during their initial treatment at the Cancer Hospital Chinese Academy of Medical Sciences, as previously described (55). Informed consent was obtained from all patients, and the samples were deidentified before use. Immunohistochemistry was performed as previously described (56). The H-scores were calculated according to the percentage of positive cells and the staining intensity as follows: H-score = Σpi × i, where pi represents the percentage of positive cells (0 to 100%) and i represents the staining intensity (0, negative; 1, weak; 2, medium; and 3, strong). IHC staining was scored by three independent pathologists. The anti-OTUB2 antibody used for IHC analysis (1:500) was provided by Dr. Long Zhang (33), and the anti-CA9 antibody used for IHC analysis (1:1,000) was purchased from Abcam (ab243660, Abcam, Cambridge, UK). Additional materials and methods are available in *SI Appendix, SI Materials and Methods*.

Data, Materials, and Software Availability. RNA-seq data have been deposited in GEO database (GSE232772) (57).

ACKNOWLEDGMENTS. We are grateful to Dr. Long Zhang (Zhejiang University, China) for providing the anti-OTUB2 antibody used for IHC staining. X.W. is supported by a National Cancer Center fellowship grant. Q.L. is supported by a Fellow grant from the Leukemia & Lymphoma Society. This study was supported by funding from the National Natural Science Foundation of China (82188102, 82030089), the National Key R&D Program of China (2021YFC2501000, 2020YFA0803300), the Chinese Academy of Medical Sciences Innovation Fund for Medical Sciences (2021-I2 M-1-018, 2021-I2 M-1-067), and the Fundamental Research Funds for the Central Universities (3332021091).

Author affiliations: [a]State Key Laboratory of Molecular Oncology, National Cancer Center/National Clinical Research Center for Cancer/Cancer Hospital, Chinese Academy of Medical Sciences and Peking Union Medical College, Beijing 100021, China; [b]Department of Cancer Biology, Dana-Farber Cancer Institute, Harvard Medical School, Boston, MA 02215; [c]Department of Genetics, Blavatnik Institute, Harvard Medical School, Boston, MA 02215; [d]Department of Medical Oncology, Dana-Farber Cancer Institute, Harvard Medical School, Boston, MA 02215; and [e]State Key Laboratory of Proteomics, National Center for Protein Sciences (Beijing), Beijing Institute of Lifeomics, Beijing 100850, China

1. H. Sung *et al.*, Global cancer statistics 2020: GLOBOCAN estimates of incidence and mortality worldwide for 36 cancers in 185 countries. *CA Cancer J. Clin.* **71**, 209–249 (2021).
2. U. Menon *et al.*, Ovarian cancer population screening and mortality after long-term follow-up in the UK Collaborative Trial of Ovarian Cancer Screening (UKCTOCS): A randomised controlled trial. *Lancet* **397**, 2182–2193 (2021).
3. D. D. Bowtell *et al.*, Rethinking ovarian cancer II: Reducing mortality from high-grade serous ovarian cancer. *Nat. Rev. Cancer* **15**, 668–679 (2015).
4. S. Zhang *et al.*, Genetically defined, syngeneic organoid platform for developing combination therapies for ovarian cancer. *Cancer Discov.* **11**, 362–383 (2021).
5. D. Hanahan, Hallmarks of cancer: New dimensions. *Cancer Discov.* **12**, 31–46 (2022).
6. D. Hanahan, R. A. Weinberg, Hallmarks of cancer: The next generation. *Cell* **144**, 646–674 (2011).
7. Y. Zhang, Y. Wang, G. Zhao, S. Orsulic, D. Matei, Metabolic dependencies and targets in ovarian cancer. *Pharmacol. Ther.* **245**, 108413 (2023).
8. G. L. Semenza, Hypoxia-inducible factor 1 (HIF-1) pathway. *Sci. STKE* **2007**, cm8 (2007).
9. A. L. Harris, Hypoxia–A key regulatory factor in tumour growth. *Nat. Rev. Cancer* **2**, 38–47 (2002).
10. A. J. Majmundar, W. J. Wong, M. C. Simon, Hypoxia-inducible factors and the response to hypoxic stress. *Mol. Cell* **40**, 294–309 (2010).
11. P. Jaakkola *et al.*, Targeting of HIF-alpha to the von Hippel-Lindau ubiquitylation complex by O2-regulated prolyl hydroxylation. *Science* **292**, 468–472 (2001).
12. J. H. Min *et al.*, Structure of an HIF-1alpha -pVHL complex: Hydroxyproline recognition in signaling. *Science* **296**, 1886–1889 (2002).
13. D. E. Foxler *et al.*, The LIMD1 protein bridges an association between the prolyl hydroxylases and VHL to repress HIF-1 activity. *Nat. Cell Biol.* **14**, 201–208 (2012).
14. J. Pouyssegur, F. Dayan, N. M. Mazure, Hypoxia signalling in cancer and approaches to enforce tumour regression. *Nature* **441**, 437–443 (2006).
15. G. Kroemer, J. Pouyssegur, Tumor cell metabolism: Cancer's Achilles' heel. *Cancer Cell* **13**, 472–482 (2008).
16. J. Chiche *et al.*, Hypoxia-inducible carbonic anhydrase IX and XII promote tumor cell growth by counteracting acidosis through the regulation of the intracellular pH. *Cancer Res.* **69**, 358–368 (2009).
17. P. C. McDonald *et al.*, Regulation of pH by carbonic anhydrase 9 mediates survival of pancreatic cancer cells with activated KRAS in response to hypoxia. *Gastroenterology* **157**, 823–837 (2019).
18. C. C. Wykoff *et al.*, Hypoxia-inducible expression of tumor-associated carbonic anhydrases. *Cancer Res.* **60**, 7075–7083 (2000).
19. K. L. Rock *et al.*, Inhibitors of the proteasome block the degradation of most cell proteins and the generation of peptides presented on MHC class I molecules. *Cell* **78**, 761–771 (1994).
20. D. Komander, M. Rape, The ubiquitin code. *Annu. Rev. Biochem.* **81**, 203–229 (2012).
21. K. N. Swatek, D. Komander, Ubiquitin modifications. *Cell Res.* **26**, 399–422 (2016).
22. J. A. Harrigan, X. Jacq, N. M. Martin, S. P. Jackson, Deubiquitylating enzymes and drug discovery: Emerging opportunities. *Nat. Rev. Drug. Discov.* **17**, 57–78 (2018).
23. B. T. Gutierrez-Diaz, W. Gu, P. Ntziachristos, Deubiquitinases: Pro-oncogenic activity and therapeutic targeting in blood malignancies. *Trends Immunol.* **41**, 327–340 (2020).
24. L. Yuan *et al.*, Deubiquitylase OTUD3 regulates PTEN stability and suppresses tumorigenesis. *Nat. Cell Biol.* **17**, 1169–1181 (2015).
25. T. Du *et al.*, The deubiquitylase OTUD3 stabilizes GRP78 and promotes lung tumorigenesis. *Nat. Commun.* **10**, 2914 (2019).
26. Q. Luo *et al.*, TRIM32/USP11 balances ARID1A stability and the oncogenic/tumor-suppressive status of squamous cell carcinoma. *Cell Rep.* **30**, 98–111.e5 (2020).
27. H. Sun *et al.*, USP11 promotes growth and metastasis of colorectal cancer via PPP1CA-mediated activation of ERK/MAPK signaling pathway. *EBioMedicine* **48**, 236–247 (2019).
28. X. Zhu *et al.*, The deubiquitinase USP11 promotes ovarian cancer chemoresistance by stabilizing BIP. *Signal Transduct. Target Ther.* **6**, 264 (2021).
29. Z. Chen *et al.*, USP9X deubiquitinates ALDH1A3 and maintains mesenchymal identity in glioblastoma stem cells. *J. Clin. Invest.* **129**, 2043–2055 (2019).
30. O. M. Khan *et al.*, The deubiquitinase USP9X regulates FBW7 stability and suppresses colorectal cancer. *J. Clin. Invest.* **128**, 1326–1337 (2018).
31. M. J. Young, K. C. Hsu, T. E. Lin, W. C. Chang, J. J. Hung, The role of ubiquitin-specific peptidases in cancer progression. *J. Biomed. Sci.* **26**, 42 (2019).
32. X. Wu *et al.*, MGMT-activated DUB3 stabilizes MCL1 and drives chemoresistance in ovarian cancer. *Proc. Natl. Acad. Sci. U.S.A.* **116**, 2961–2966 (2019).
33. Z. Zhang *et al.*, OTUB2 promotes cancer metastasis via hippo-independent activation of YAP and TAZ. *Mol. Cell* **73**, 7–21.e7 (2019).
34. W. Chang *et al.*, OTUB2 exerts tumor-suppressive roles via STAT1-mediated CALML3 activation and increased phosphatidylserine synthesis. *Cell Rep.* **41**, 111561 (2022).
35. J. T. Buters *et al.*, Cytochrome P450 CYP1B1 determines susceptibility to 7, 12-dimethylbenz[a] anthracene-induced lymphomas. *Proc. Natl. Acad. Sci. U.S.A.* **96**, 1977–1982 (1999).
36. M. C. Hollander *et al.*, Dimethylbenzanthracene carcinogenesis in Gadd45a-null mice is associated with decreased DNA repair and increased mutation frequency. *Cancer Res.* **61**, 2487–2491 (2001).
37. P. H. Maxwell *et al.*, The tumour suppressor protein VHL targets hypoxia-inducible factors for oxygen-dependent proteolysis. *Nature* **399**, 271–275 (1999).
38. J. Li *et al.*, OTUB2 stabilizes U2AF2 to promote the Warburg effect and tumorigenesis via the AKT/mTOR signaling pathway in non-small cell lung cancer. *Theranostics* **9**, 179–195 (2019).
39. G. Liu, W. Guo, J. Qin, Z. Lin, OTUB2 facilitates tumorigenesis of gastric cancer through promoting KDM1A-mediated stem cell-like properties. *Front. Oncol.* **11**, 711735 (2021).
40. S. Ouyang *et al.*, OTUB2 regulates KRT80 stability via deubiquitination and promotes tumour proliferation in gastric cancer. *Cell Death Discov.* **8**, 45 (2022).
41. S. Yu, W. Zang, Y. Qiu, L. Liao, X. Zheng, Deubiquitinase OTUB2 exacerbates the progression of colorectal cancer by promoting PKM2 activity and glycolysis. *Oncogene* **41**, 46–56 (2022).
42. M. D. Brooks *et al.*, Human calmodulin-like protein CALML3: A novel marker for normal oral squamous mucosa that is downregulated in malignant transformation. *Int. J. Dent.* **2013**, 592843 (2013).
43. R. D. Bennett, M. R. Pittelkow, E. E. Strehler, Immunolocalization of the tumor-sensitive calmodulin-like protein CALML3 in normal human skin and hyperproliferative skin disorders. *PLoS One* **8**, e62347 (2013).

44. C. Zhan *et al.*, Identification of immunohistochemical markers for distinguishing lung adenocarcinoma from squamous cell carcinoma. *J. Thorac. Dis.* **7**, 1398–1405 (2015).
45. J. Martin *et al.*, The sequence and analysis of duplication-rich human chromosome 16. *Nature* **432**, 988–994 (2004).
46. D. S. Gerhard *et al.*, The status, quality, and expansion of the NIH full-length cDNA project: The Mammalian Gene Collection (MGC). *Genome Res.* **14**, 2121–2127 (2004).
47. O. Warburg, The metabolism of carcinoma cells. *J. Cancer Res.* **9**, 148–163 (1925).
48. W. H. Koppenol, P. L. Bounds, C. V. Dang, Otto Warburg's contributions to current concepts of cancer metabolism. *Nat. Rev. Cancer* **11**, 325–337 (2011).
49. P. S. Ward, C. B. Thompson, Metabolic reprogramming: A cancer hallmark even warburg did not anticipate. *Cancer Cell* **21**, 297–308 (2012).
50. U. E. Martinez-Outschoorn, M. Peiris-Pages, R. G. Pestell, F. Sotgia, M. P. Lisanti, Cancer metabolism: A therapeutic perspective. *Nat. Rev. Clin. Oncol.* **14**, 11–31 (2017).
51. X. Song *et al.*, JTC801 induces pH-dependent death specifically in cancer cells and slows growth of tumors in mice. *Gastroenterology* **154**, 1480–1493 (2018).
52. E. S. Silagi, E. Schipani, I. M. Shapiro, M. V. Risbud, The role of HIF proteins in maintaining the metabolic health of the intervertebral disc. *Nat. Rev. Rheumatol.* **17**, 426–439 (2021).
53. S. Sobhanifar, C. Aquino-Parsons, E. J. Stanbridge, P. Olive, Reduced expression of hypoxia-inducible factor-1alpha in perinecrotic regions of solid tumors. *Cancer Res.* **65**, 7259–7266 (2005).
54. P. C. McDonald *et al.*, A phase 1 study of SLC-0111, a novel inhibitor of carbonic anhydrase IX, in patients with advanced solid tumors. *Am. J. Clin. Oncol.* **43**, 484–490 (2020).
55. T. Shu, Y. Li, X. Wu, B. Li, Z. Liu, Down-regulation of HECTD3 by HER2 inhibition makes serous ovarian cancer cells sensitive to platinum treatment. *Cancer Lett.* **411**, 65–73 (2017).
56. Q. Luo *et al.*, OTUD1 activates caspase-independent and caspase-dependent apoptosis by promoting AIF nuclear translocation and MCL1 degradation. *Adv. Sci. (Weinh)* **8**, 2002874 (2021).
57. Y. Nan, X. Wu, Q. Luo, W. Chang, Data from "OTUB2 silencing promotes ovarian cancer via mitochondrial metabolic reprogramming and can be synthetically targeted by CA9 inhibition." GEO. Available at https://www.ncbi.nlm.nih.gov/geo/query/acc.cgi?acc=GSE232772. Deposited 18 May 2023.